Journal of Controlled Release 183 (2014) 114–123

Contents lists available at ScienceDirect

Journal of Controlled Release

journal homepage: www.elsevier.com/locate/jconrel

Phosphatidylserine-targeted bimodal liposomal nanoparticles for *in vivo* imaging of breast cancer in mice

Liang Zhang [a], Heling Zhou [a], Olivier Belzile [b], Philip Thorpe [b], Dawen Zhao [a,*]

[a] Radiology, UT Southwestern Medical Center, Dallas, USA
[b] Pharmacology, UT Southwestern Medical Center, Dallas, USA

ARTICLE INFO

Article history:
Received 14 February 2014
Accepted 24 March 2014
Available online 1 April 2014

Keywords:
Phosphatidylserine (PS)
Bimodal liposomal nanoprobe
Tumor vasculature
Magnetic resonance imaging (MRI)
Near-infrared optical imaging
Breast cancer

ABSTRACT

Phosphatidylserine (PS) that is normally constrained to the inner plasma membrane becomes exposed on the surface of endothelial cells (ECs) in tumor vasculature. In the present study, we report the development of a novel tumor vasculature-targeted liposomal nanoprobe by conjugating a human monoclonal antibody, PGN635 that specifically targets PS to polyethylene glycol-coated liposomes. MR contrast, superparamagnetic iron oxide nanoparticles (SPIO) were packed into the core of liposomes, while near-infrared dye, DiR was incorporated into the lipophilic bilayer. The liposomal nanoprobe PGN-L-IO/DiR was fully characterized, and its binding specificity and subsequent internalization into PS-exposed vascular ECs was confirmed by *in vitro* MRI and histological staining. *In vivo* longitudinal MRI and optical imaging were performed after i.v. injection of the liposomal nanoprobes into mice bearing breast MDA-MB231 tumors. At 9.4 T, T_2-weighted MRI detected drastic reduction on signal intensity and T_2 values of tumors at 24 h. Ionizing radiation significantly increased PS exposure on tumor vascular ECs, resulting in a further MRI signal loss of tumors. Concurrent with MRI, optical imaging revealed a clear tumor contrast at 24 h. Intriguingly, PGN-L-IO/DiR exhibited distinct pharmacokinetics and biodistribution with significantly reduced accumulations in liver or spleen. Localization of PGN-L-IO/DiR to tumor was antigen specific, since a control probe of irrelevant specificity showed minimal accumulation in the tumors. Our studies indicate that PS-targeted liposomes may provide a useful platform for tumor-targeted delivery of imaging contrast agents or potentially anti-cancer drugs for cancer theranostics.

1. Introduction

Solid tumors are well known for their ability to grow in the harsh microenvironment characterized by hypoxia, acidosis and oxidative stress. All these factors contribute significantly to genetic and epigenetic instability in tumor cells as well as tumor stromal cells. Studies by Thorpe's lab have demonstrated that the oxidative stress within tumor microenvironment causes redistribution of phosphatidylserine (PS), the most abundant anionic phospholipid of the cell membrane, from the inner to the outer membrane leaflet of tumor endothelial cells (ECs; Schemes in Fig. 1a) [1,2]. These cells are actually found to be viable and not subject to apoptotic process. PS exposure on tumor ECs is inducible and reversible [3,4]. The cells can resume growth and reestablish phospholipid asymmetry, which is distinct from the irreversible process occurring in cell death [4,5]. Examinations of a large panel of tumor types including prostate, breast, lung and brain tumors grown in mice and rats have exhibited that PS exposure on tumor ECs is universal, despite the extent of exposure varying between the tumor types [6–10]. In normal mammalian cells, even in those highly angiogenic ovarian blood vessels during ovulation, PS is asymmetrically distributed across the plasma membrane with essentially all the PS localized in the cell's inner membrane. Thus, PS exposed on tumor but not normal vascular endothelial cells creates a highly specific biomarker for tumor vasculature. A fully human monoclonal PS-targeting antibody, PGN635 has recently been developed. PGN635 binds to PS complexed with the PS-binding protein, β2-glycoprotein I (β2GP1) with a higher specificity and affinity to PS (kD ≈ 10^{-10} M), as compared to annexin V [10–12].

We have previously utilized PGN635 to develop a PS-targeted near infrared fluorescence probe to facilitate *in vivo* optical imaging of glioma in mouse models [10]. Successful visualization of glioma grown in mouse brain provides the proof of principle that PS-targeted imaging probes may be useful for sensitive tumor detection. MRI is the most commonly used imaging modality in clinical oncology, with high spatial resolution and excellent soft tissue contrast. MRI has recently been recommended by the American Cancer Society for breast cancer screening as an adjunct to mammography [13]. However, with the traditional contrast agent, gadolinium, MRI of breast cancer is still encountering the challenges of low sensitivity and specificity. Thus, development of

* Corresponding author at: Department of Radiology, UT Southwestern Medical Center, 5323 Harry Hines Blvd., Dallas, TX 75390-9058, USA. Tel.: +1 214 648 9621; fax: +1 214 648 4538.
E-mail address: Dawen.Zhao@UTSouthwestern.edu (D. Zhao).

http://dx.doi.org/10.1016/j.jconrel.2014.03.043
0168-3659/

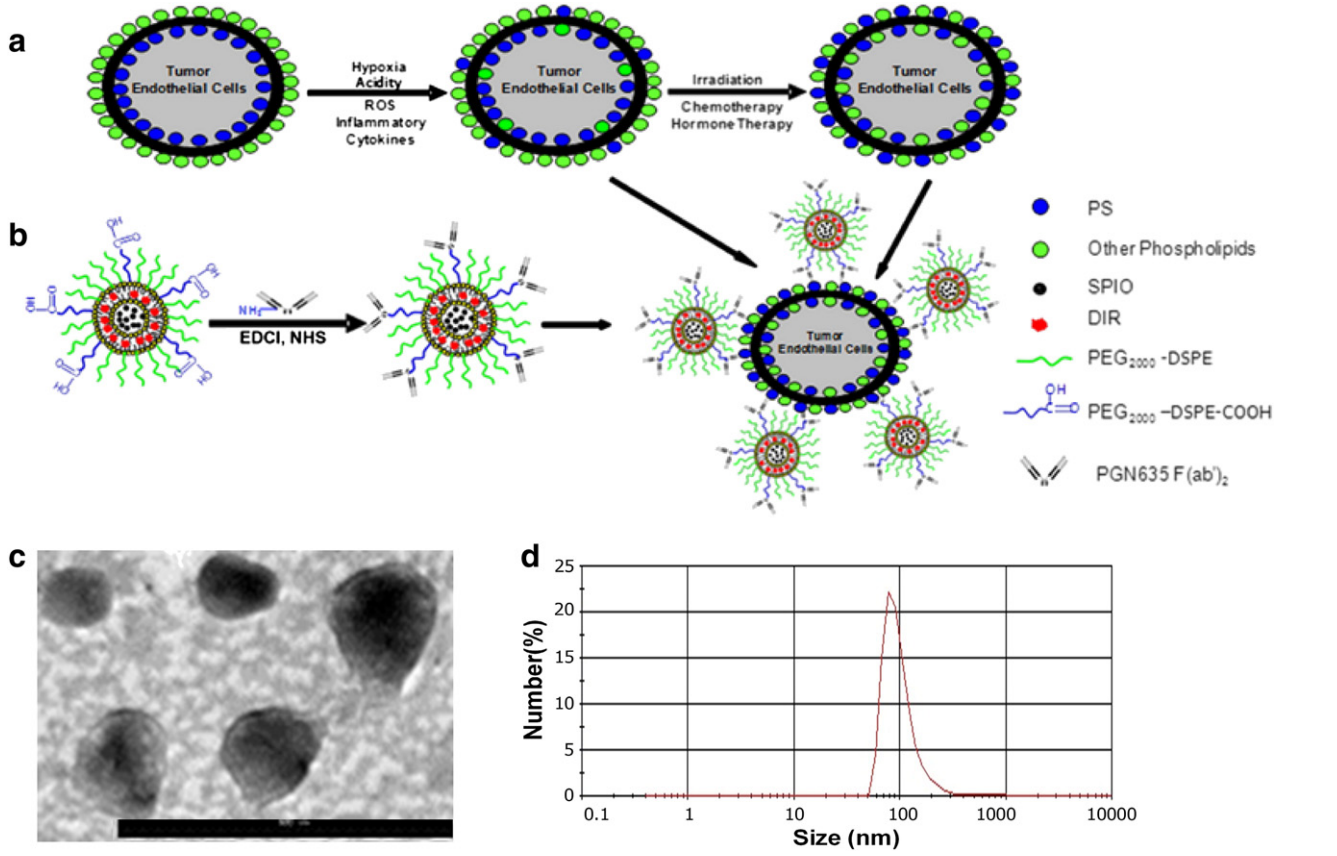

Fig. 1. PS exposure on tumor vascular endothelium targeted specifically by bimodal liposomal nanoprobes. Schematic illustrations: a. PS exposure specifically on tumor vascular endothelial cells, and b. Preparation of liposome loaded with MRI and optical bimodal contrast and functionalized with PGN635F(ab′)$_2$ that bind to exposed PS. c. A representative transmission electron microscopic (TEM) image (bar = 500 nm) of PGN-L-IO/DiR enclosing SPIO in their cores. d. A size distribution curve obtained by dynamic light scattering (DLS) analysis indicates an average hydrodynamic size of PGN-L-IO/DiR = 111 nm.

breast cancer-targeted molecular imaging probes may help to improve the sensitive and specific detection of breast cancer at an early stage.

Many efforts have been made to improve delivery of chemotherapeutics or imaging agents to tumors. Liposome-based nanocarriers have been widely applied for such molecular transport because of their capacity of a large payload and the protective bilayers shielding the enclosed molecules from interaction with the contents of the blood stream [14,15]. By coating the liposomal surface with PEG-polymers, the circulation time of liposomes can be significantly prolonged and thus increased efficacy can be achieved [16,17]. Liposomes are also known for their preference for tumor accumulation due to the enhanced permeation and retention (EPR) effect [18]. However, the selectivity based upon the EPR effect has been demonstrated to vary significantly both intra- and inter-tumorally due to the heterogeneous nature of tumors [19,20]. Thus, functionalization of liposomes with tumor-specific targeting moieties will be essential to achieve enhanced tumor selectivity [20–22].

In this study, we utilized liposomes as nanocarriers to develop PS-targeted dual MRI/optical imaging nanoprobes, PGN-L-IO/DiR. MR contrast, superparamagnetic iron oxide nanoparticles (SPIO, 10 nm in diameter) were entrapped inside the aqueous cores, while near infrared dye, DiR (absorption/emission wavelength: 748/780 nm) was incorporated into the bilayers of liposomes. We then conjugated the F(ab′)$_2$ fragments of PGN635 to the carboxyl groups on the distal terminus of PEG chains that are coated on the surface of liposomes (Schemes in Fig. 1b). PGN-L-IO/DiR nanoprobes were fully characterized and their binding specificity to exposed PS was studied *in vitro* by MRI and histological staining. *In vivo* dual MRI/optical imaging was performed to longitudinally monitor changes in tumor contrast after i.v. injection of PGN-L-IO/DiR into mice bearing human breast MDA-MB231 tumors. Ionizing radiation that is known to induce oxidative stress was used to increase PS exposure on vascular ECs and tumor cells. MDA-MB231 tumors after irradiation were imaged to reveal enhanced tumor contrast due to increased PS binding of PGN-L-IO/DiR. Distribution of PGN-L-IO/DiR nanoprobes in normal organs was also evaluated by *in vivo* MRI and *ex vivo* optical imaging. Superior tumor uptakes and significantly reduced liver and spleen accumulations compared to the control liposomal probes further indicate the highly specific tumor targeting of PGN-L-IO/DiR.

2. Material and methods

2.1. Preparation and characterization of PS-targeted liposomes loaded with MRI and optical imaging contrast

The procedure used for preparation of liposomes has been described previously [23]. In brief, egg phosphatidylcholine (EPC) (Sigma-Aldrich Corporation, MO), cholesterol (Sigma-Aldrich Corporation, MO), 1,2-distearoyl-sn-glycero-3-phosphoethanolamine-N-[methoxy(polyethylene glycol)$_{2000}$] (PEG$_{2000}$–DSPE), 1,2-distearoyl-sn-glycero-3-phosphoethanolamine-N-[carboxy(polyethylene glycol)$_{2000}$] (COOH-PEG$_{2000}$-DSPE) (Avanti Polar Lipids, Alabaster, AL) and 1,1′-dioctadecyl-3,3,3′,3′-tetramethyl indotricarbocyanine Iodide (DiR, Perkin-Elmer, Waltham, MA) were dissolved in chloroform (53:45:4:1:0.8 μmol/μmol) in a pear-shaped flask. The lipid film was prepared by removing the chloroform using a rotary vacuum evaporator. The rough DiR plus SPIO liposomes were produced by hydration of the film with PBS containing SPIO (10 nm, Ocean Nanotech, AR) with sonication in water bath for 5 min, followed by sonication using a probe-type sonicator (Omni International Inc., Kennesaw, GA) for 5 min. The sample was centrifuged at 1000 *g* for

15 min at 4 °C to precipitate the free SPIO. Unencapsulated DiR in the supernatant was further removed by using a DynaMag™ (Invitrogen, Grand Island, NY) magnetic separator overnight at 4 °C. The DiR plus SPIO liposomes were suspended and extruded through polycarbonate membranes with 400 nm and then 200 nm pore sizes (Nalgene, Rochester, NY). The content of SPIO in the liposomes was determined by the atomic absorption spectrometer (Varian Medical Systems, USA), and the content of DiR in the liposomes was determined by the microplate reader (Molecular Devices, Sunnyvale, CA). The encapsulation efficiency (EE) of SPIO or DiR was determined based on the formula: $EE = (W_{encap} / W_{total}) \times 100\%$, where W_{encap} is the measured amount of SPIO or DiR in the liposomal suspensions, W_{total} is the total amount of SPIO or DiR used initially.

To functionalize the bimodal liposomes with PS-targeting antibody, the human monoclonal antibody PGN635 that was generated by Affitech A.S. (Oslo, Norway) in collaboration with Peregrine Pharmaceuticals. Inc. (Tustin, CA) was used. Aurexis is a human monoclonal antibody that binds to an irrelevant antigen (*Staphylococcus aureus* clumping factor A) and was used as a negative control antibody. PGN635 and Aurexis $F(ab')_2$ fragments were generated by reacting antibodies with pepsin at a molar ratio of 1:130 (antibody:pepsin) for 1 h at 37 °C. $F(ab')_2$ fragments (MW = 110 kD) were purified by FPLC using an S-200 column (Pharmacia, Piscataway, NJ) and PBS running buffer. PGN635 $F(ab')_2$ or aurexis $F(ab')_2$ were then conjugated to the distant terminus of polyethylene glycol (PEG) chain coated liposomes. Briefly, 3.52 μmol of 1-(3-dimethylaminopropyl)-3-ethylcarbodiimide hydrochloride (EDC, Sigma-Aldrich) and 7.88 μmol of N-hydroxysuccinimide (NHS, Sigma-Aldrich) were added into 2 ml of DiR and SPIO loaded liposomes ($COOH\text{-}PEG_{2000}$-DSPE:EDCI:NHS = 0.02:3.52:7.88, μmol/μmol; pH 7.4) and gently stirred for 30 min at room temperature. PGN635 $F(ab')_2$ or aurexis $F(ab')_2$ (PGN635 $F(ab')_2$ or aurexis $F(ab')_2$: $COOH\text{-}PEG_{2000}$-DSPE = 1:2, μmol/μmol) were then added into the suspensions and allowed to continuously react for 5 h at room temperature. Excess EDC and NHS were removed by dialysis. The liposome suspensions were applied to a quick spin Sephadex G-50 column (Fisher Scientific, Pittsburg, PA) equilibrated with PBS and centrifuged at 150 *g* at 4 °C to remove the uncoupled antibodies. Subsequently, liposome fractions were collected from quick spin Sephadex G-50 column, and the content of antibodies on the liposomes was determined by both bicinchoninic acid (BCA) assay and Bradford protein assay (Sigma-Aldrich). The modifying rate (MR) of antibody was calculated with the formula: $MR = (W_{modifying}{}^{\circ} / W_{total}) \times 100\%$, where $W_{modifying}$ is the measured amount of antibody in the liposomes after passing over the column, while W_{total} is the total amount of antibodies added. The nanoprobes are referred to as PGN-L-IO/DiR or the control, Aur-L-IO/DiR throughout the text.

The mean diameter and zeta potential of the liposome nanoprobes were measured by dynamic light scattering (DLS) analysis with Zetasizer 3000HSA (Malvern Instruments Ltd., U.K.). The morphological shapes were observed using a transmission electron microscope (TEM, JEM-1230, JEOL, Japan). Finally, the stability of the nanoprobes was evaluated using a simple filtration test. In brief, PGN-L-IO/DiR or Aur-L-IO/DiR in PBS (pH 7.4) containing 10% fetal bovine serum were incubated for 48 h at 37 °C. 100 ml of each solution was continuously passed through syringe filter membranes (Nalgene, USA) with different pore sizes of 0.80, 0.45, and 0.22 μm at 0 h, 24 h and 48 h, respectively. Near infrared fluorescence (NIRF) images of each sample before/after the filtration test were observed using a Maestro imaging system (CRi, Inc., Woburn, MA).

2.2. In vitro cytotoxicity

Adult bovine aortic endothelial cells (ABAE; Clonetics, Walkersville, MD) were cultured in DMEM medium (Sigma-Aldrich) supplemented with 10% fetal bovine serum (Invitrogen), 100 units/ml penicillin (Sigma-Aldrich), and 100 units/ml streptomycin (Sigma-Aldrich). Cytotoxicity of PGN-L-IO/DiR was assessed by using the trypan blue staining assay. ABAE cells were seeded into 6-well culture plates at a density of 2.8×10^5 cells per well and grown in culture medium in the incubator at 37 °C. PGN-L-IO/DiR or the control Aur-L-IO/DiR were added into 6-well culture plates containing SPIO of 0–200 μg/ml, respectively. The survival rate was determined at 48 h by 0.4% trypan blue staining, and the number of viable cells were measured by an automated cell counter (Bio-Rad, Hercules, CA).

2.3. In vitro binding specificity

Adult bovine aortic endothelial (ABAE) cells were used. To induce PS exposure, the cells were treated with a single dose of 6 Gy X-radiation. Twenty-four hours later, the irradiated cells were incubated with PGN-L-IO/DiR or the control Aur-L-IO/DiR at a concentration of 29 μg/ml iron for 1 h. For the blocking study, the cells were pretreated with the full length PGN635 for 1 h prior to PGN-L-IO/DiR. Unbound particles were washed away with PBS, and then the cells were fixed with 4% paraformaldehyde [24]. Immunocytochemistry and Prussian blue staining were performed to detect the specific binding of PGN-L-IO/DiR to PS-exposed cells. Moreover, the PGN-L-IO/DiR or Aur-L-IO/DiR treated ABAE cells (3×10^5) were mixed homogeneously with 0.8% agarose and fast spin echo multi-slice (FSEMS) T_2-weighted images (TR = 3000 ms, effective TE ranging from 40 to 120 ms with a 20 ms increment, average = 2, number of slices = 10, acquisition time = 10 min) were acquired using a 9.4 T horizontal bore magnet. Both T_2-weighted SI and T_2 values of each agarose mixture were quantified.

2.4. Tumor model

All animal procedures were approved by the Institutional Animal Care and Use Committee of University of Texas Southwestern Medical Center. MDA-MB231 cells (3×10^6) in 100 μl of serum-free medium containing 25% Matrigel (BD Biosciences, San Jose, CA) were injected subcutaneously on a thigh or both thighs of anesthetized mice (n = 19; BALB/c nu/nu, 6–8 weeks old; NCI, Frederick, MD). Animals were sedated with 3% isoflurane and maintained under general anesthesia (2% isoflurane).

2.5. Detection and quantification of exposed PS in MDA-MB231 tumors

When subcutaneous tumors on both thighs reached 6–8 mm in diameter, a single dose of 12 Gy of irradiation was delivered to the tumors on the right thigh using a small animal irradiator (XRAD320; Precision X-ray, Inc., North Branford, CT) fitted with a variable collimator to generate a single adjustable collimated iso-dose beam of X-rays at a dose rate of 10 Gy/min. Twenty-four hours later, 150 μg of PGN635 or the control body Aurexis was injected i.v. and allowed to circulate for 4 h. The mice were anesthetized, exsanguinated, and perfused with heparinized saline. The tumors on both sides were removed and frozen for preparation of cryosections. Vascular endothelium was stained using a rat anti-mouse CD31 antibody (BD Biosciences, San Jose, CA) followed by Cy3-labeled goat anti-rat IgG. PGN635 or Aurexis was detected using goat anti-human IgG conjugated to Cy2. Doubly labeled endothelial cells (*i.e.* CD31 positive/PGN635 positive) were identified by yellow fluorescence on merged images. The percentage of doubly positive vessels was calculated as follows: (mean number of yellow vessels per field/mean number of total vessels) × 100. Ten random 0.079-mm^2 fields were evaluated for each section.

2.6. In vivo MRI and optical imaging of tumor targeted PGN-L-IO/DiR nanoprobes

Human breast cancer MDA-MB231 cells were implanted subcutaneously on a thigh of nude mice (n = 6). When tumors grew to 5 mm in diameter, T_2-weighted FSEMS MRI at 9.4 T was acquired before and at different time points after i.v. injection of PGN-L-IO/DiR or the control

Aur-L-IO/DiR. Immediately after MRI at 24 h, near infrared fluorescence imaging was performed and repeated at 48 h using Maestro imaging system [24]. For irradiation study, the tumor cells were implanted on both thighs, one of which received a focal radiation with a single dose of 12 Gy. Twenty-four hours later, the MRI and optical imaging procedures, as described above, were conducted to detect changes in signal intensity in both irradiated and non-irradiated tumors after i.v. injection of PGN-L-IO/DiR ($n = 6$) or the control Aur-L-IO/DiR ($n = 4$). For MRI data, T_2-weighted SI in tumors *versus* thigh muscles as well as absolute T_2 relaxation time of tumors were quantified for each time point post i.v. injection of the liposomal nanoprobes and compared with the pre-injection baseline values. For optical imaging analysis, average photon counts normalized by time (s) in tumors and adjacent normal skin were obtained. TNR was used for quantifying dynamic changes in signal intensity.

2.7. Ex vivo optical imaging of biodistribution

Immediately after *in vivo* imaging at 48 h post injection, the tumor-bearing mice were sacrificed. Major organs and tumor tissues were dissected and subjected to optical imaging [25]. Average photon counts was obtained for tumors and each organ/tissue and normalized by the muscle value.

2.8. Histological and immunohistochemical studies

For fluorescence microscopy, cryosections of tumor tissues were immunostained with antibodies against the endothelial marker, CD31 and followed by Cy2-conjugated secondary antibody. The near infrared signals of DiR were recorded and merged with the CD31 image and the DAPI-stained image of the same field. To detect SPIO, Prussian blue staining was performed on the sections pre-stained with anti-CD31 and followed by horseradish peroxidase (HRP)-conjugated goat anti rat secondary antibody.

2.9. Statistical analysis

Analysis of MRI data was performed on a home written MATLAB program on both pixel-by-pixel and region of interest (ROI) basis [25]. ROIs were drawn on both the tumors and adjacent thigh muscles on the high resolution T_2-weighted images. Signal intensity (SI) in these ROIs was measured for all the echoes of FSEMS images and a ratio of tumor to muscle (TMR) was obtained. One-way ANOVA analysis of variance was used to determine significance among groups, after which post hoc tests with the Bonferroni correction were used for multiple comparisons between individual groups.

3. Results

3.1. Characteristics of PGN-L-IO/DiR

The bimodal liposomal nanoprobes were characterized with respect to particle size, charge, encapsulation efficiency (EE) and antibody coupling efficiency (BCA assay), as illustrated in Table 1 and Fig. 1. Percentage calculation of EE of PGN-L-IO/DiR was also obtained for SPIO ($56.83 \pm 2.39\%$), DiR ($98.61 \pm 1.11\%$) and antibody ($85.91 \pm 6.42\%$). Before conjugation, the polydispersity index (PDI) of PEG coated liposomes was 0.11 ± 0.03, as compared to the PDI $= 0.12 \pm 0.01$ for PGN-L-IO/DiR (Table 1). Consistent with the results of the BCA assay, the Bradford protein assay detected a $87.65\% \pm 6.61$ (10.77 ± 0.81 nmol/mg lipid) and $86.63\% \pm 8.58$ (10.64 ± 1.05 nmol/mg lipid) antibody coupling efficiency for PGN-L-IO/DiR and Aur-L-IO/DiR, respectively. MRI relaxivity of PGN-L-IO/DiR was obtained at 9.4 T: $r_1 = 0.35\ mM^{-1}\ s^{-1}$; $r_2 = 163\ mM^{-1}\ s^{-1}$, indicating it as a strong T_2 contrast agent. Stability and toxicity studies were also performed, showing that the liposomes were stable in serum for at least 48 h and minimally toxic to adult bovine aorta endothelial (ABAE) cells (Suppl. Fig. 1).

3.2. In vitro studies of PS-targeting specificity of PGN-L-IO/DiR

Under normal culture conditions, there is essentially no PS exposed ABAE cell. To induce exposure of PS on the outer membrane of the cells, ABAE cells were irradiated 24 h earlier with a single dose of 6 Gy. Immunocytochemical (Fig. 2a–d) and Prussian blue staining (Fig. 2e–h) revealed specific binding of PGN-L-IO/DiR to PS exclusively in the irradiated cells (Fig. 2c, g and h), but not in the non-irradiated cells (Fig. 2a and e). Both DiR signal (Fig. 2c) and positive iron staining (Fig. 2g and h) were detected in cytoplasm. The control Aur-L-IO/DiR did not bind to PS-exposed cells (Fig. 2b and f). Specificity of PGN-L-IO/DiR was further confirmed by pre-incubating with non-labeled PGN635 to block the binding of PGN-L-IO/DiR (Fig. 2d). The targeting and multimodal-imaging capability was also tested by *in vitro* MRI (Fig. 2i and j). In a good agreement with the histological data, T_2-weighted MRI visualized signal darkness in the irradiated cells treated with PGN-L-IO/DiR and the maximal reduction of signal intensity (SI) was observed at the highest iron concentration (52 μg/ml). Measurements of T_2 relaxation time showed significant reduction of T_2 values for the irradiated cells incubated with various concentrations of PGN-L-IO/DiR ($p < 0.05$; Fig. 2j). No significant changes in SI or T_2 values were observed for the cells treated with the control Aur-L-IO/DiR or pre-treated with the non-labeled antibodies (Fig. 2i and j).

3.3. Detection and quantification of exposed PS in MDA-MB231 tumors

An average of $20 \pm 8\%$ of blood vessels in non-irradiated tumors had exposed PS on their endothelium, as judged by coincident staining of vessels by PGN635 and anti-CD31 (Fig. 3a). Twenty-four hours after a single dose of 12 Gy radiation, PGN635 binding was significantly increased, indicating increased levels of exposed PS in the tumors. PGN635 staining localized on both vascular endothelial cells ($50 \pm 8\%$; $p < 0.001$; Fig. 3b) and tumor cells (Fig. 3).

3.4. In vivo longitudinal MRI and optical imaging of PGN-L-IO/DiR in breast cancer MDA-MB231 xenografts

3.4.1. In vivo MRI

Longitudinal MRI was performed on the MDA-MB231 tumor bearing mice ($n = 6$) before and after i.v. injection of PGN-L-IO/DiR (2.5 mg/kg iron). As shown in Fig. 4a, certain tissue inhomogeneity was observed in the tumors on T_2-weighted images prior to injection. However, 24 h post injection, massive intratumoral hypointense regions appeared. Longitudinal SI changes showed that decrease in tumor SI was gradual and slow during the first 8 h (11% decrease at 8 h), but then became steeper and reached 63% of the preinjection level at 24 h (37% decrease;

Table 1
Characteristics of bimodal liposomes functionalized with antibody fragments.

Nanoprobe	DiR loaded (μg)/lipid (mg)	SPIO loaded (μg)/lipid (mg)	Antibody modified (nmol)/lipid (mg)	Mean size (nm)	Zeta potential (mV)	Polydispersity index, PDI
PGN-L-IO/DiR	19.64 ± 0.22	71.04 ± 2.99	10.55 ± 0.79	111.23 ± 4.77	−3.67 ± 0.22	0.12 ± 0.01
Aur-L-IO/DiR	18.72 ± 1.09	67.34 ± 2.45	10.51 ± 1.59	114.60 ± 6.61	−3.37 ± 0.24	0.13 ± 0.01

Data are presented as the mean ± standard deviation. Each assay was repeated thrice.
EE: encapsulation efficiency.

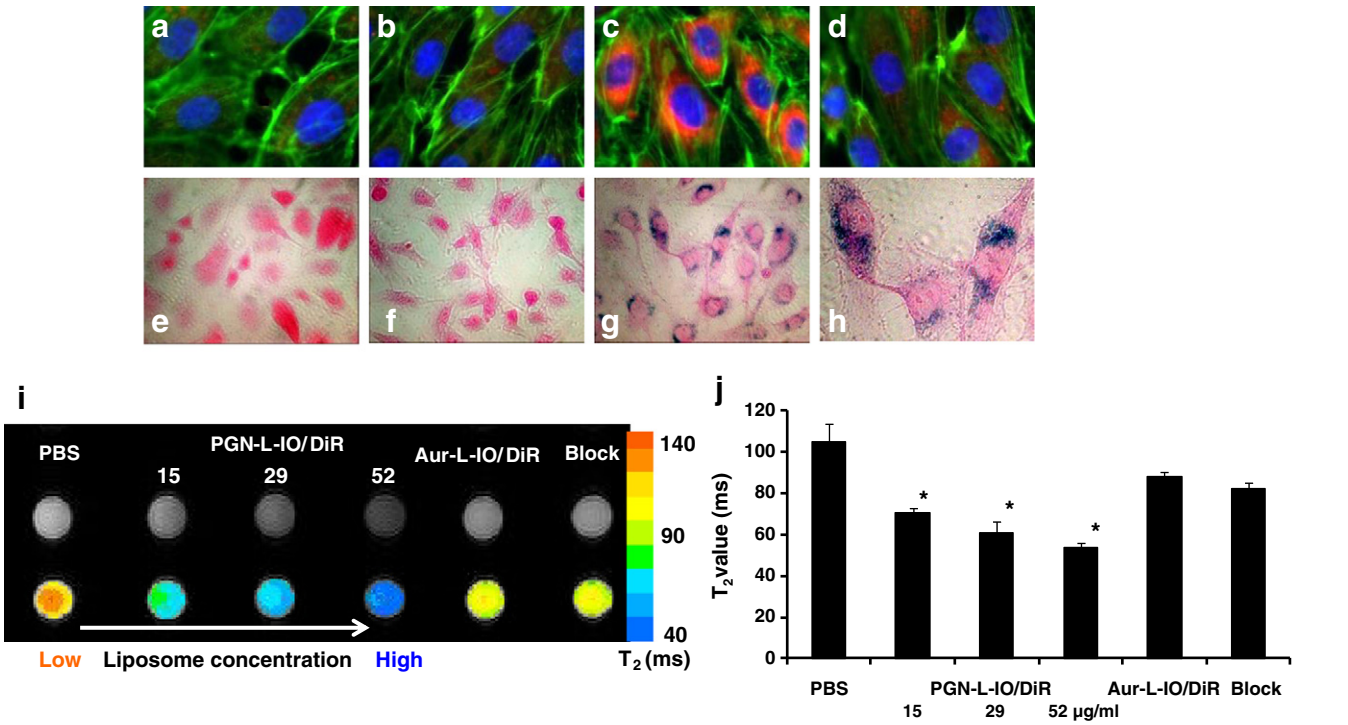

Fig. 2. *In vitro* specificity studies of bimodal PGN-L-IO/DiR nanoprobes. Top: Immunocytochemistry (a–d) and Prussian blue staining of ABAE ECs pretreated with/without radiation of a 6 Gy. 24 h later, the cells were incubated with either PGN-L-IO/DiR or the control Aur-L-IO/DiR for 1 h before fixation and subsequent staining. a–d, Merged fluorescence images showed minimal DiR (red) signals from non-irradiated cells (a) or Aur-L-IO/DiR treated irradiated cells (b). By contrast, massive cytoplasmic DiR signals were seen in the PGN-L-IO/DiR-treated irradiated cells (c). Prior treatment with the full length PGN635 blocked majority of DiR signals (d). Note: green: cytoskeleton actin; blue: nuclei. e–h, Similar results were observed by Prussian blue staining that blue iron staining was only seen in the irradiated cells treated with PGN-L-IO/DiR (g), but not in the non-irradiated cells (e) or Aur-L-IO/DiR treated cells (f). h. A region of g was magnified to clearly show intracellular localization of PGN-L-IO/DiR. Bottom: *In vitro* MRI measurements of T_2-weighted signal intensity and T_2 values in the agarose phantom of ABAE cells. i. Signal intensity on T_2-weighted images of the irradiated cells decreases with increased concentrations of PGN-L-IO/DiR, consistent with the decreased T_2 values. Specific binding of PGN-L-IO/DiR was blocked by unlabeled PGN635 antibodies. Quantitative T_2 values (mean ± SD) showed significant reduction on T_2 values of the PGN-L-IO/DiR ($^*p < 0.05$; j).

Fig. 4b). By contrast, the liver had an acute signal drop in the first 4 h but then a slower slope afterwards (Fig. 4b). Quantitative analysis of T_2 values of the tumors treated with PGN-L-IO/DiR in Fig. 4c and d indicated a significant decrease in T_2 at 24 h (mean = 39 ± 2 ms), as compared to the pretreatment (51 ± 1 ms; $p < 0.05$).

3.4.2. In vivo near infrared optical imaging

Immediately after MRI at 24 h, the mice were imaged with optical imaging of DiR. As presented in Fig. 4e, a clear tumor contrast was seen at 24 h and sustained at 48 h in the mouse used for the MRI studies in Fig. 4a–d. The mean tumor/normal ratio (TNR; n = 6) was 6.3 ± ±.4 at 24 h and 5.9 ± 0.8 at 48 h. In addition, a subset of tumor bearing mice (n = 3) were subjected to longitudinal optical imaging to determine the kinetics of tumor uptake of PGN-L-IO/DiR (Suppl. Fig. 2). In common with the MRI data, significant increase in light signal was detected at 24 h post PGN-L-IO/DiR ($p < 0.01$; Suppl. Fig. 2).

3.5. MRI/optical imaging of irradiation-enhanced PS exposure

The above mentioned longitudinal MRI/optical procedures were applied to the mice bearing two thigh tumors 24 h after the right tumor received 12 Gy radiation. For the non-irradiated tumors, the time course and magnitude changes of MRI and optical signals were consistent with those of the single tumor studies as shown above. As expected, irradiation significantly enhanced PS exposure, resulting in more PGN-L-IO/DiR binding than that in the non-irradiated tumor. Like the non-irradiated tumors, signal changes in MRI/optical imaging were significant at 24 h post i.v. PGN-L-IO/DiR. MRI measurements of T_2 of the irradiated tumors revealed an average of 27 ± ±% decrease from the baseline level, which was significantly higher than a 14 ± ±% decrease for the non-irradiated tumors (Fig. 5a, b and e; $p < 0.05$). Similarly, significantly enhanced tumor contrast was seen for the irradiated (TNR = 9.3 ± 0.7) *vs.* non-irradiated (TNR = 4.2 ± 1.5; $p < 0.05$) by optical imaging of DiR signal. Compared to specific tumor-targeting of PGN-L-IO/DiR, the control antibody conjugates, Aur-L-IO/DiR showed minimal changes in T_2 of MRI and optical signal (Fig. 5c, d and f; $p < 0.05$).

3.6. Ex vivo optical imaging of biodistribution of PGN-L-IO/DiR

Ex vivo optical imaging of the excised tumors and normal tissues and organs confirmed that the irradiated tumors had the highest fluorescence signal (mean tumor/muscle ratio (TMR) = 26 ± 7), which was significantly higher than that of the liver or spleen ($p < 0.05$; Fig. 6a and b). The non-irradiated tumor had a mean TMR = 10 ± 4, while other major organs such as kidney and lung had minimal uptakes of the nanoprobes. By contrast, the control Aur-L-IO/DiR was predominantly detected in spleen and liver (TMR = 33 and 28, respectively). Either irradiated or non-irradiated tumors had minimal accumulation of the control probes (TMR = 5 and 3, respectively; Fig. 6b). Observations of significantly reduced accumulation of the targeted probes in the reticuloendothelial system (RES) of liver and spleen further suggest that the highly tumor-specific binding of PGN-L-IO/DiR may alter their pharmacokinetics and biodistribution.

3.7. Histological and immunohistochemical analysis

Fluorescence immunohistochemical staining and Prussian blue staining confirmed abundant DiR and iron particles in the non-irradiated and irradiated tumors of the mice injected with PGN-L-IO/DiR (Fig. 6c). Co-localizations of the nanoprobes with tumor vascular

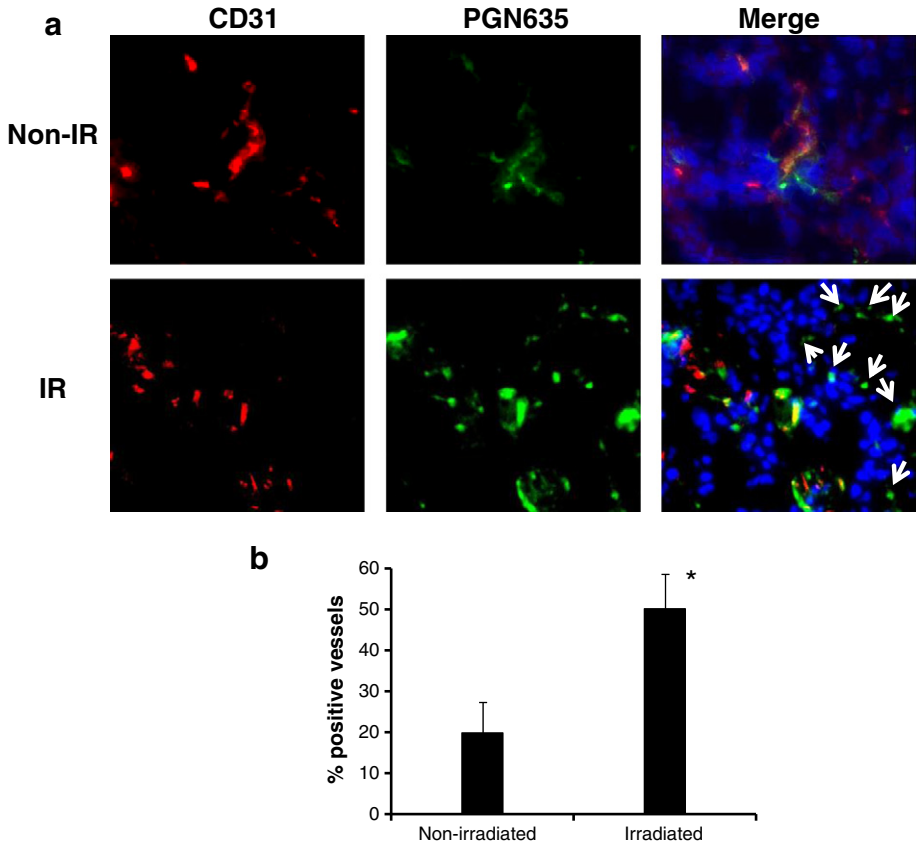

Fig. 3. Immunohistochemical study of localization of PGN635 antibody in non-irradiated and irradiated tumors. Mice bearing a subcutaneous MDA-MB231 tumor on each thigh received a single dose of 12 Gy irradiation to the right side tumor. Exposure of PS was determined 24 h later by i.v. injection of full length PGN635. Animals were perfused with saline 4 h later. a. Frozen sections of non-irradiated and irradiated tumors were analyzed for the presence of PGN635 (green). Vascular endothelial cells were counterstained with anti-CD31 (red). Merged images revealed coincidence of staining showing that PGN635 was bound to vascular ECs in the non-irradiated tumor. Increased PGN635 staining was seen in the irradiated tumors and was due to increased staining of both endothelial cells and tumor cells (arrows). b. Irradiation increased the percentage of PS-positive vessels from 20 ± 7(SD) % to 50 ± 8 (SD) % ($p < 0.001$).

endothelial cells (anti-CD31) were evidenced by both stainings. Significantly less DiR and iron was seen in the tumors treated with the control Aur-L-IO/DiR, validating the specificity of tumor-targeted PGN-L-IO/DiR.

4. Discussion

We have demonstrated in this study that bimodal liposomal nanoprobes functionalized with PS-targeted antibody fragments are highly sensitive and specific, allowing dual MRI/optical imaging to detect the enhanced tumor contrast in breast tumor xenografts owing to PGN-L-IO/DiR binding to PS exposed tumor vessels. *In vitro* binding assay clearly revealed extensive cytoplasmic localizations of PGN-L-IO/DiR in the PS-exposed cells. Specificity of PGN-L-IO/DiR was also confirmed by using the control Aur-L-IO/DiR that showed minimal uptake in the PS exposed cells. Moreover, observations of dose-dependent uptakes and the diminishing binding with the competition study were further supportive. *In vivo* binding of PGN-L-IO/DiR to PS exposed tumor vascular ECs was successfully visualized by both MRI and optical imaging after i.v. injection of the nanoprobes. Consistent imaging data from both imaging modalities showed no significant tumor uptakes of the nanoprobes by 8 h post injection. Irradiation significantly increased PS exposure in tumor vascular ECs and tumor cells, resulting in enhanced tumor contrast. Intriguingly, accumulations of PGN-L-IO/DiR in reticuloendothelial system (RES) of liver and spleen, were found to be significantly reduced.

Ideally, cancer imaging probes are desired to target exclusively to cancer-specific markers with a high affinity [26–28]. Cell surface biomarkers, in particular, those on tumor vascular endothelial cells are attractive targets because they are the most readily accessible target sites. Antibodies, antibody derivatives or peptides against tumor vascular specific antigens have been extensively studied for their ability to facilitate cancer molecular imaging. Applications of $\alpha v\beta 3$ binding ligands, such as Arginine-Glycine-Aspartic Acid (RGD)-containing peptides have been successful in tumor imaging. RGD-based imaging probes have been developed for optical imaging, PET, SPECT and MRI of tumor angiogenesis in both preclinical and clinical settings [29–32]. In this study, we have utilized a fully human monoclonal antibody, PGN635 to target PS exposed on tumor vascular ECs. PS is strictly located in the inner leaflet of the plasma membrane bilayer in normal cells, including the vascular endothelium. Cell surface-exposed PS is thereby an attractive target for tumor molecular imaging. Whole antibodies that expose their constant regions, Fc are more susceptible to Fc-receptor-mediated phagocytosis. Thus, the $F(ab')_2$ fragments of PGN635 (MW ≈ 110 kD) were prepared and used in this study. Different tumors were reported to vary in the percentage of their vessels that have exposed PS [1,2,6–8]. In Dunning R3227-AT1 prostate tumors, as high as 40% of vessels have exposed PS [8]. Similar to our current data of MDA-MB231 tumors, our previous study of U87 gliomas showed that the percentage of tumor vessels that had exposed PS increased from 27% to 64% after irradiation with 12 Gy [10].

Liposomes have become useful drug delivery vehicles because of their ability to carry a large payload of drugs or imaging moieties either entrapped in their core or bilayer without chemically modifying them. Another advantage of liposomal drugs over free drugs is that liposomes with surface coating of PEG-polymers have significantly longer

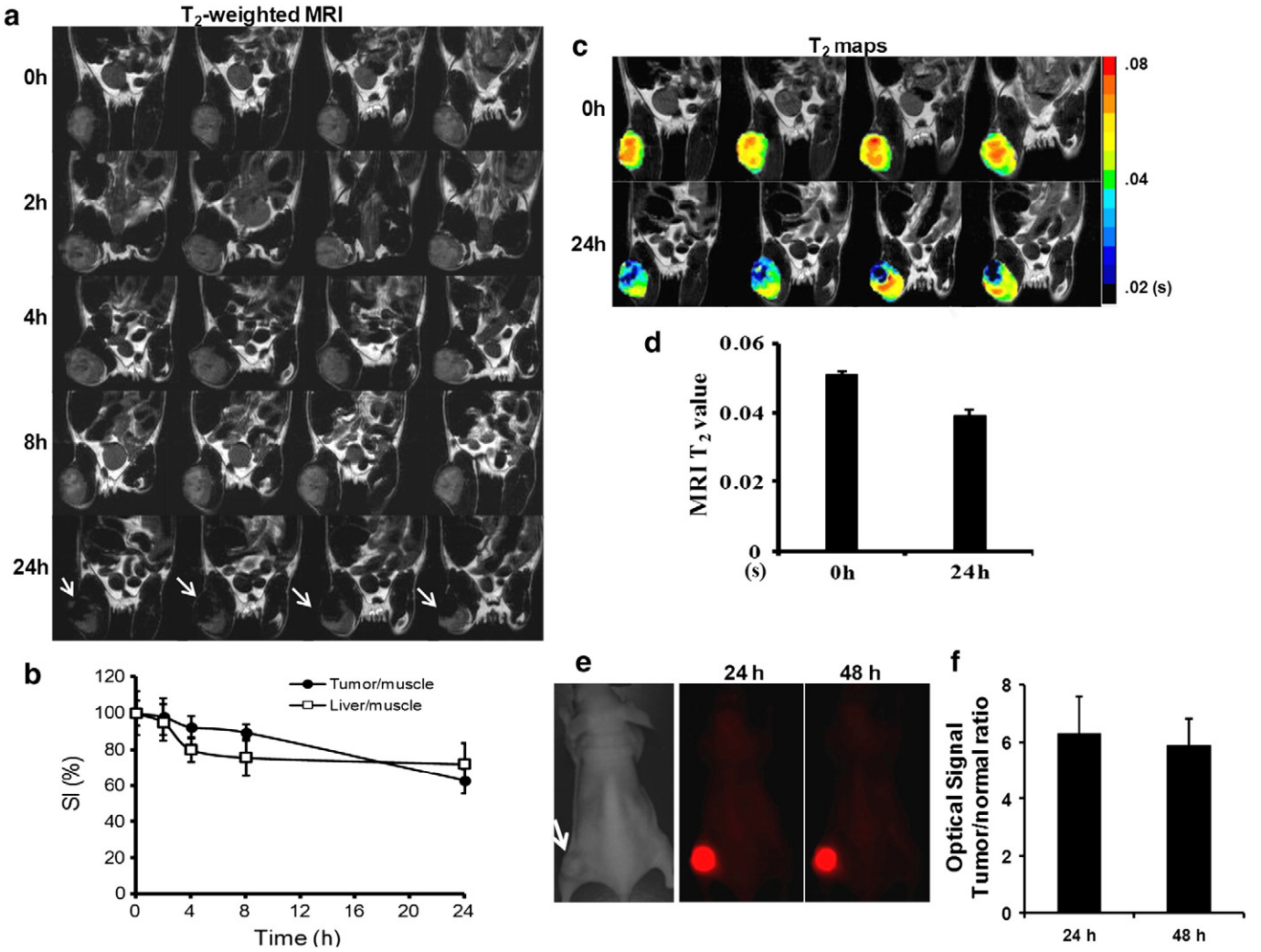

Fig. 4. *In vivo* MRI and optical imaging of exposed PS in MDA-MB231 breast tumors. a. Representative T_2-weighted fast spin echo multi-slice images were acquired before and at different time points post injection of PGN-L-IO/DiR (2.5 mg Fe/kg) *via* a tail vein of a mouse bearing a subcutaneous tumor. 24 h post injection, intratumoral signal voids were clearly seen on all the four consecutive slices of the tumor. b. The ratio of SI of tumor *versus* adjacent thigh muscle was obtained, and the average ratio at each time point post PGN-L-IO/DiR was normalized to that of pre-injection. Similarly, the ratio of liver to muscle was calculated. The time course curves showed decrease in SI in both tumor and liver post PGN-L-IO/DiR. c. T_2 maps of pre- and 24 h post injection were created, revealing decreased T_2 values at 24 h. d. Quantitative T_2 measurements showed a significant reduction on T_2 at 24 h (39 ± 2 (SD) ms), as compared to the baseline value of 51 ± 1 ms ($p < 0.05$). e. Immediately after MRI at 24 h, the same mouse was subjected to optical imaging. A clear optical contrast was seen in the tumor and sustained by 48 h after injection. f. The mean TNR was 6.3 ± 1.4 (SD) at 24 h and 5.9 ± 0.8 at 48 h.

circulation time. This is believed to be attributed in part to their selective tumor accumulations *via* the EPR effect. However, vascular permeability in tumors varies with respect to tumor type. In the current study of breast MDA-MB231 tumors, the control antibody labeled liposomes showed less noticeable accumulations in the tumors (Figs. 5 and 6). Thus, it is imperative to functionalize the liposome with active targeting moieties to obtain a higher level of liposome accumulation. Indeed, significantly enhanced tumor uptakes were achieved in this study by conjugating PS-targeted monoclonal antibody fragments to the surface of liposomes. Targeting the luminal surface-exposed PS obviates the need for extravasation of the nanoprobes from blood vessels. The imaging data of PGN-L-IO/DiR were in good agreement with previous studies of PGN635 F(ab′)$_2$ labeled imaging probes by us [10,33] and others [34,35]. Our previous study of the near-infrared optical probe, 800CW-PGN635 F(ab′)$_2$ showed a similar time course of optical signal intensity change in the non-irradiated U87 gloma of a mouse model, in which significantly enhanced tumor contrast was obtained only at 24 h [10]. However, the two probes differed with respect to the magnitude of optical signal change. The maximal TNR of the non-irradiated and irradiated tumors in this study were 4.2 and 9.3, respectively (Fig. 5f), which were a twofold increase as compared to those of the 800CW probes in U87 gliomas. The enhanced tumor contrast seen with the liposomal nanoprobes may be associated with the high payload of optical contrast agents. Moreover, an increased number of PGN635F(ab′)$_2$ bound on each liposome, as compared to a single antibody to a 800CW molecule, could increase the avidity of their binding to PS exposed cells.

We have previously shown that the full length PS-targeting antibody bavituximab labeled with arsenic-74 (^{74}As, $t_{1/2}$ = ~18 days) gave clear PET images of prostate tumors in rats with the optimal imaging time at 72 h after injection. In a recent study, Stafford et al. reported that iodine-124 (^{124}I, $t_{1/2}$ = ~4 days) labeled PGN635 F(ab′)$_2$ had a maximal PET imaging signal at 24 h post injection [34]. PGNF(ab′)$_2$ did indeed allow for more rapid imaging of tumors than the full length antibody. However, the longer blood half-life of ^{125}I-PGN635 F(ab′)$_2$ than that of the control Aurexis F(ab′)$_2$ was observed in the biodistribution study. The difference is most likely due to the generation of PGN635 F(ab′)$_2$/β2GP1 complexes that are cleared significantly more slowly than that of Aurexis F(ab′)$_2$ [34]. Utilization of smaller antibody fragments, *i.e.*, single chain variable fragment (scFv) or short amino acid peptides has also been investigated extensively, aiming to achieve faster imaging of tumors. Zhang et al. have recently shown that SPIO functionalized with integrin $\alpha_v\beta_3$-targeting cyclic Arg-Gly-Asp (cRGD) enabled clear

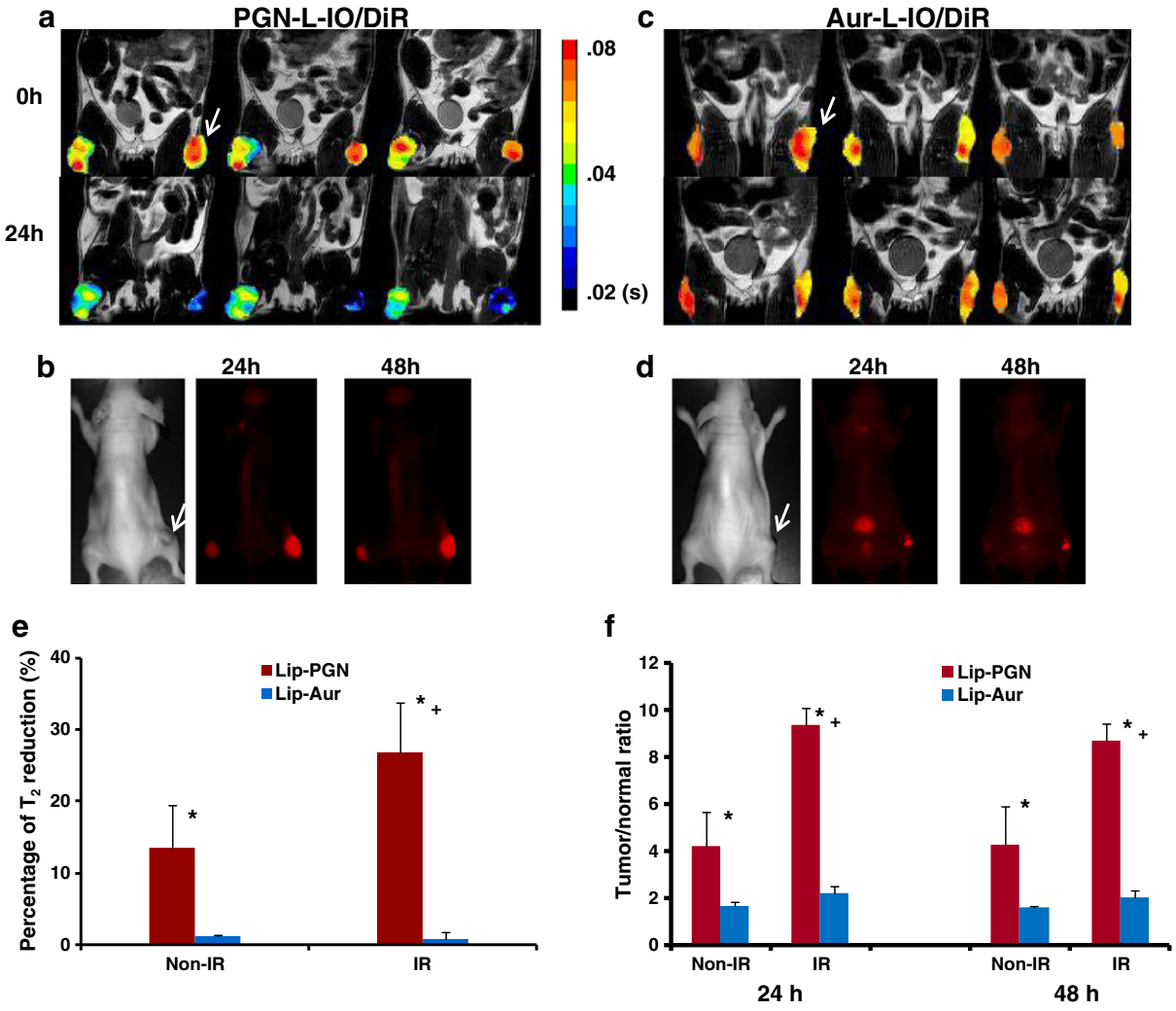

Fig. 5. *In vivo* bimodal imaging of radiation-enhanced PS exposure in MDA-MB231 breast tumors. a. A representative mouse bearing size-matched subcutaneous tumors on each thigh received 12 Gy of irradiation to the right side tumor. 24 h after radiation, PGN-L-IO/DiR was injected *via* a tail vein. T_2 maps showed T_2 shortening of both the non-irradiated and irradiated tumor at 24 h post injection, as compared to the baseline. Irradiation increased the level of PS exposure, resulting in a further decrease on T_2. b. Consistent with MRI data, optical imaging revealed a brighter signal in the irradiated tumor. c and d. By contrast, minimal accumulation of Aur-L-IO/DiR was detected in either the irradiated tumor or the non-irradiated tumor. e. Statistical analysis showed a mean of 13% decrease on T_2 of the non-irradiated tumors ($n = 6$) at 24 h post PGN-L-IO/DiR, as compared to a 1% reduction in the Aur-L-IO/DiR tumors ($n = 4$; $^*p < 0.05$). Significantly more reduction on T_2 was found for the irradiated tumors post PGN-L-IO/DiR ($n = 6$, mean decrease $= 27 \pm 6$ (SD) %; $^+p < 0.05$). f. Similarly, optical imaging detected a significantly higher TNR in the PGN-L-IO/DiR groups (4.2 ± 1.5 (SD) at 24 h and 4.3 ± 1.7 at 48 h) than the Aur-L-IO/DiR groups (1.6 ± 0.2 at 24 h and 1.6 ± 0.1 at 48 h; $^*p < 0.05$). Irradiation significantly increased the TNR to 9.3 ± 0.7 at 24 h and 8.7 ± 0.7 at 48 h ($+p < 0.05$).

tumor contrast at 6 h post injection [36]. Compared to the small fragments of antibody or peptides, the full length or $F(ab')_2$ dimers of antibody are generally considered to have higher binding affinity. Moreover, non-specific uptakes by liver and spleen are often problematic for other PS binding molecules, *i.e.*, annexin V, labeled imaging probes. The exact mechanism is not fully understood, but is probably due, at least in part, to nonspecific RES system in liver and spleen to capture and metabolize low molecular weight proteins [34]. Advantageous biodistribution of the PGN635 $F(ab')_2$ labeled imaging probes that were significantly less accumulated in normal organs as evidenced in the current study and earlier studies further suggests its usefulness for cancer imaging [10,34,35].

One interesting observation in the current study was that PGN-L-IO/DiR bound to cell surface-exposed PS and then became internalized in the cytoplasm of cells (Fig. 2). This is contradictory to previous reports that the PS antibodies–β2GP1-PS complex remains on the external cell membrane for a few days before the macrophages recognize and clear them out [7,12]. Likewise, conjugates of the antibodies with optical imaging contrast agents in our previous study were found not to be internalized [10]. Our recent unpublished data have also shown exclusive external cell membrane localizations of MRI probes of SPIO (20 nm)-PGN635$F(ab')_2$. The distinguishing feature of liposomal nanoprobes may result from the fusion of the lipid layers between liposomes and cells after PGN635 bound to PS on cell membrane. In fact, it has been reported that targeting ligands on the surface of liposomes leads to the binding, close apposition, and fusion of the lipid layer with the targeted cell lipid membrane [37,38]. Subsequently, the contents of the liposomes enter the cells and may eventually be excreted into the extravascular extracellular space. However, the exact mechanisms for the internalization of PGN-L-IO/DiR as well as the fate of the nanoprobes still need further investigation, which will provide valuable information to extend the utilization of the PS-targeted liposomal nanocarriers for theranostic applications.

In addition to sensitive detection of specific tumor targeting, MRI provided spatial information about intratumoral localization of PS-target nanoprobes. Unlike the relatively homogeneous signal enhancement seen by optical imaging, MRI revealed heterogeneous T_2-weighted signal loss and T_2 reduction (Figs. 4 and 5). In contrast to the T_1 contrast agent, gadolinium-DTPA, SPIO is a T_2 contrast agent, which generates negative contrast on T_2 or T_2^*-weighted images. In

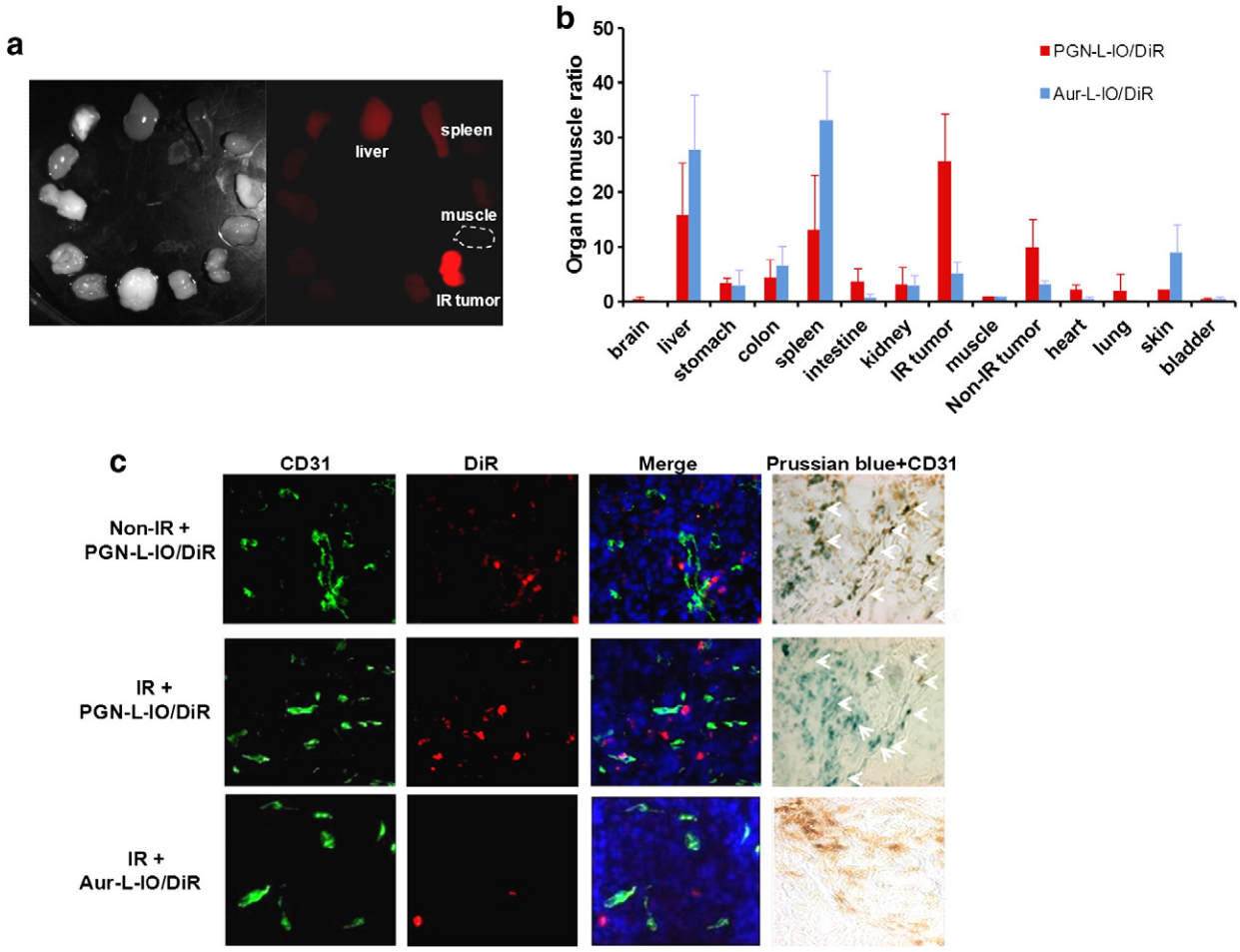

Fig. 6. *Ex vivo* optical imaging of biodistribution of PGN-L-IO/DiR and microscopic imaging of localization of PGN-L-IO/DiR in tumors. a. Immediately after *in vivo* optical imaging at 48 h, *ex vivo* optical imaging was performed and average photon counts were obtained for tumors and normal organs and normalized by the muscle value. b. For the mice injected with PGN-L-IO/DiR, the highest TMR of 26 was seen for the irradiated tumors, while liver and spleen had a mean of 16 and 13, respectively. The non-irradiated tumor had a mean TMR of 10. For the Aur-L-IO/DiR group, large amounts of the probes were found in spleen (mean = 33) and liver (mean = 28). Irradiated and non-irradiated tumors had a mean TMR of 5 and 3, respectively. c. Fluorescence microscopy was applied to detect DiR signals, and Prussian blue staining for iron nanoparticles. Sections of non-irradiated or irradiated tumors were immunofluorescently examined for the presence of DiR (red), CD31 (green) or DAPI. The merged image showed that the PGN-L-IO/DiR nanoprobes localized not only on the vascular endothelial cells but also on the tumor cells. More DiR appeared in the irradiated tumors. By contrast, little DiR was seen in the Aur-L-IO/DiR control tumors. Similarly, double staining of Prussian blue and anti CD31 (brown) revealed the localization of PGN-L-IO/DiR on both vascular ECs (arrows) and tumor cells.

comparison to paramagnetic T_1 contrast, SPIO has much higher molar relaxivity, thus, it is widely used for molecular imaging applications by MRI [39,40].

Irradiation increased PS exposure in MDA-MB231 tumors from 20% to 50% (Fig. 3), resulting in significantly increased binding of PGN-L-IO/DiR, detected by both MRI and optical imaging (Fig. 5). In addition to tumor vasculature, a single dose of 12 Gy radiation also caused loss of PS asymmetry in some tumor cells. Much interest has been generated in developing molecular imaging probes that enable noninvasive monitoring of the response of patients' tumors to various treatments that induce tumor apoptosis [41,42]. Annexin V is the PS binding ligand that is most widely used for this purpose [43,44]. In addition to PS, annexin V also binds to other anionic phospholipids and phosphatidylethanolamine (PE). PGN635 and bavituximab, a chimeric monoclonal antibody that is currently being evaluated in clinical trials [40], have a more restricted specificity for PS. We believe that PGN-L-IO/DiR nanoprobes have the potential for imaging of tumor response to treatment.

5. Conclusion

In summary, we have developed a PS-targeted bimodal liposomal nanoprobe and demonstrated its usefulness for sensitive *in vivo* imaging of breast MDA-MB231 tumors in mice. Excellent tumor contrast after i.v. infusion of PGN-L-IO/DiR was visualized by both MRI and optical imaging. MRI was able to provide spatial information about intratumoral distribution of the nanoprobes. Our data showed that PGN-L-IO/DiR nanoparticles were antigen specific and had significantly reduced liver and spleen uptake. Liposomes have proven promising in the delivery of chemotherapeutic agents, and currently they are being applied in the clinical treatment of cancer patients. Given its distinct characteristics of internalization and favorable biodistribution, it will be feasible to incorporate both imaging and therapeutic agents into the PS-targeted liposomal platform, ultimately enabling non-invasive monitoring of tumor location, tumor targeting levels, intratumoral drug distribution and therapeutic response in cancer patients.

Acknowledgments

This work was supported in part by DOD W81XWH-12-1-0317. Imaging was conducted by DOE grant DE-FG02-05CH11280, NIH BTRP P41-RR02584, NCI U24 CA126608 and NCI 1P30 CA142543. Dr. Philip Thorpe was a key investigator being both on discovering exposed PS on tumor vasculature and development of a series of PS-targeting antibodies. Sadly he passed away shortly after the completion of the study.

We thank Peregrine Pharmaceuticals Inc., Tustin, CA, for the provision of PGN635 antibody. We are grateful to Drs. Yiguang Wang, Gang Huang and Jinming Gao for technical and collegial support.

Appendix A. Supplementary data

Supplementary data to this article can be found online at http://dx.doi.org/10.1016/j.jconrel.2014.03.043.

References

[1] S. Ran, A. Downes, P.E. Thorpe, Increased exposure of anionic phospholipids on the surface of tumor blood vessels, Cancer Res. 62 (2002) 6132–6140.
[2] S. Ran, P.E. Thorpe, Phosphatidylserine is a marker of tumor vasculature and a potential target for cancer imaging and therapy, Int. J. Radiat. Oncol. Biol. Phys. 54 (2002) 1479–1484.
[3] A.K. Hammill, J.W. Uhr, R.H. Scheuermann, Annexin V staining due to loss of membrane asymmetry can be reversible and precede commitment to apoptotic death, Exp. Cell Res. 251 (1999) 16–21.
[4] B. Mirnikjoo, K. Balasubramanian, A.J. Schroit, Mobilization of lysosomal calcium regulates the externalization of phosphatidylserine during apoptosis, J. Biol. Chem. 284 (2009) 6918–6923.
[5] K. Balasubramanian, A.J. Schroit, Aminophospholipid asymmetry: a matter of life and death, Annu. Rev. Physiol. 65 (2003) 701–734.
[6] J. He, T.A. Luster, P.E. Thorpe, Radiation-enhanced vascular targeting of human lung cancers in mice with a monoclonal antibody that binds anionic phospholipids, Clin. Cancer Res. 13 (2007) 5211–5218.
[7] J. He, Y. Yin, T.A. Luster, L. Watkins, P.E. Thorpe, Antiphosphatidylserine antibody combined with irradiation damages tumor blood vessels and induces tumor immunity in a rat model of glioblastoma, Clin. Cancer Res. 15 (2009) 6871–6880.
[8] M. Jennewein, M.A. Lewis, D. Zhao, E. Tsyganov, N. Slavine, J. He, L. Watkins, V.D. Kodibagkar, S. O'Kelly, P. Kulkarni, P.P. Antich, A. Hermanne, F. Rosch, R.P. Mason, P.E. Thorpe, Vascular imaging of solid tumors in rats with a radioactive arsenic-labeled antibody that binds exposed phosphatidylserine, Clin. Cancer Res. 14 (2008) 1377–1385.
[9] J.H. Stafford, P.E. Thorpe, Increased exposure of phosphatidylethanolamine on the surface of tumor vascular endothelium, Neoplasia 13 (2011) 299–308.
[10] D. Zhao, J.H. Stafford, H. Zhou, P.E. Thorpe, Near-infrared optical imaging of exposed phosphatidylserine in a mouse glioma model, Transl. Oncol. 4 (2011) 355–364.
[11] S. Ran, J. He, X. Huang, M. Soares, D. Scothorn, P.E. Thorpe, Antitumor effects of a monoclonal antibody that binds anionic phospholipids on the surface of tumor blood vessels in mice, Clin. Cancer Res. 11 (2005) 1551–1562.
[12] T.A. Luster, J. He, X. Huang, S.N. Maiti, A.J. Schroit, P.G. de Groot, P.E. Thorpe, Plasma protein beta-2-glycoprotein 1 mediates interaction between the anti-tumor monoclonal antibody 3G4 and anionic phospholipids on endothelial cells, J. Biol. Chem. 281 (2006) 29863–29871.
[13] D. Saslow, C. Boetes, W. Burke, S. Harms, M.O. Leach, C.D. Lehman, E. Morris, E. Pisano, M. Schnall, S. Sener, R.A. Smith, E. Warner, M. Yaffe, K.S. Andrews, C.A. Russell, American Cancer Society guidelines for breast screening with MRI as an adjunct to mammography, CA Cancer J. Clin. 57 (2007) 75–89.
[14] V.P. Torchilin, Recent advances with liposomes as pharmaceutical carriers, Nat. Rev. Drug Discov. 4 (2005) 145–160.
[15] F. Pastorino, C. Brignole, D. Marimpietri, P. Sapra, E.H. Moase, T.M. Allen, M. Ponzoni, Doxorubicin-loaded Fab′ fragments of anti-disialoganglioside immunoliposomes selectively inhibit the growth and dissemination of human neuroblastoma in nude mice, Cancer Res. 63 (2003) 86–92.
[16] A.L. Klibanov, K. Maruyama, V.P. Torchilin, L. Huang, Amphipathic polyethyleneglycols effectively prolong the circulation time of liposomes, FEBS Lett. 268 (1990) 235–237.
[17] A.A. Gabizon, Pegylated liposomal doxorubicin: metamorphosis of an old drug into a new form of chemotherapy, Cancer Invest. 19 (2001) 424–436.
[18] H. Maeda, T. Sawa, T. Konno, Mechanism of tumor-targeted delivery of macromolecular drugs, including the EPR effect in solid tumor and clinical overview of the prototype polymeric drug SMANCS, J. Control. Release 74 (2001) 47–61.
[19] D. Peer, J.M. Karp, S. Hong, O.C. Farokhzad, R. Margalit, R. Langer, Nanocarriers as an emerging platform for cancer therapy, Nat. Nanotechnol. 2 (2007) 751–760.
[20] T.L. Andresen, S.S. Jensen, K. Jorgensen, Advanced strategies in liposomal cancer therapy: problems and prospects of active and tumor specific drug release, Prog. Lipid Res. 44 (2005) 68–97.
[21] J.W. Park, D.B. Kirpotin, K. Hong, R. Shalaby, Y. Shao, U.B. Nielsen, J.D. Marks, D. Papahadjopoulos, C.C. Benz, Tumor targeting using anti-her2 immunoliposomes, J. Control. Release 74 (2001) 95–113.
[22] P. Sapra, T.M. Allen, Internalizing antibodies are necessary for improved therapeutic efficacy of antibody-targeted liposomal drugs, Cancer Res. 62 (2002) 7190–7194.
[23] L. Zhang, H.J. Yao, Y. Yu, Y. Zhang, R.J. Li, R.J. Ju, X.X. Wang, M.G. Sun, J.F. Shi, W.L. Lu, Mitochondrial targeting liposomes incorporating daunorubicin and quinacrine for treatment of relapsed breast cancer arising from cancer stem cells, Biomaterials 33 (2012) 565–582.
[24] D. Sturm, H. Witt, V. Hovestadt, D.A. Khuong-Quang, D.T. Jones, C. Konermann, E. Pfaff, M. Tonjes, M. Sill, S. Bender, M. Kool, M. Zapatka, N. Becker, M. Zucknick, T. Hielscher, X.Y. Liu, A.M. Fontebasso, M. Ryzhova, S. Albrecht, K. Jacob, M. Wolter, M. Ebinger, M.U. Schuhmann, T. van Meter, M.C. Fruhwald, H. Hauch, A. Pekrun, B. Radlwimmer, T. Niehues, G. von Komorowski, M. Durken, A.E. Kulozik, J. Madden, A. Donson, N.K. Foreman, R. Drissi, M. Fouladi, W. Scheurlen, A. von Deimling, C. Monoranu, W. Roggendorf, C. Herold-Mende, A. Unterberg, C.M. Kramm, J. Felsberg, C. Hartmann, B. Wiestler, W. Wick, T. Milde, O. Witt, A.M. Lindroth, J. Schwartzentruber, D. Faury, A. Fleming, M. Zakrzewska, P.P. Liberski, K. Zakrzewski, P. Hauser, M. Garami, A. Klekner, L. Bognar, S. Morrissy, F. Cavalli, M.D. Taylor, P. van Sluis, J. Koster, R. Versteeg, R. Volckmann, T. Mikkelsen, K. Aldape, G. Reifenberger, V.P. Collins, J. Majewski, A. Korshunov, P. Lichter, C. Plass, N. Jabado, S.M. Pfister, Hotspot mutations in H3F3A and IDH1 define distinct epigenetic and biological subgroups of glioblastoma, Cancer Cell 22 (2012) 425–437.
[25] M. Demeule, D. Shedid, E. Beaulieu, R.F. Del Maestro, A. Moghrabi, P.B. Ghosn, R. Moumdjian, F. Berthelet, R. Beliveau, Expression of multidrug-resistance P-glycoprotein (MDR1) in human brain tumors, Int. J. Cancer 93 (2001) 62–66.
[26] R. Weissleder, M.J. Pittet, Imaging in the era of molecular oncology, Nature 452 (2008) 580–589.
[27] L. Yang, X.H. Peng, Y.A. Wang, X. Wang, Z. Cao, C. Ni, P. Karna, X. Zhang, W.C. Wood, X. Gao, S. Nie, H. Mao, Receptor-targeted nanoparticles for *in vivo* imaging of breast cancer, Clin. Cancer Res. 15 (2009) 4722–4732.
[28] D. Artemov, Molecular magnetic resonance imaging with targeted contrast agents, J. Cell. Biochem. 90 (2003) 518–524.
[29] W. Cai, X. Chen, Multimodality molecular imaging of tumor angiogenesis, J. Nucl. Med. 49 (Suppl. 2) (2008) 113S–128S.
[30] D.A. Sipkins, D.A. Cheresh, M.R. Kazemi, L.M. Nevin, M.D. Bednarski, K.C. Li, Detection of tumor angiogenesis *in vivo* by alphaVbeta3-targeted magnetic resonance imaging, Nat. Med. 4 (1998) 623–626.
[31] C. Khemtong, C.W. Kessinger, J. Ren, E.A. Bey, S.G. Yang, J.S. Guthi, D.A. Boothman, A.D. Sherry, J. Gao, *In vivo* off-resonance saturation magnetic resonance imaging of alphavbeta3-targeted superparamagnetic nanoparticles, Cancer Res. 69 (2009) 1651–1658.
[32] A.P. Pathak, M.F. Penet, Z.M. Bhujwalla, MR molecular imaging of tumor vasculature and vascular targets, Adv. Genet. 69 (2010) 1–30.
[33] L. Zhang, D. Zhao, Liposomal encapsulation enhances *in vivo* near infrared imaging of exposed phosphatidylserine in a mouse glioma model, Molecules 18 (2013) 14613–14628.
[34] J.H. Stafford, G. Hao, A.M. Best, X. Sun, P.E. Thorpe, Highly specific PET imaging of prostate tumors in mice with an iodine-124-labeled antibody fragment that targets phosphatidylserine, PLoS One 8 (2013) e84864.
[35] A. Ogasawara, J.N. Tinianow, A.N. Vanderbilt, H.S. Gill, S. Yee, J.E. Flores, S.P. Williams, A. Ashkenazi, J. Marik, ImmunoPET imaging of phosphatidylserine in pro-apoptotic therapy treated tumor models, Nucl. Med. Biol. 40 (2013) 15–22.
[36] C. Zhang, M. Jugold, E.C. Woenne, T. Lammers, B. Morgenstern, M.M. Mueller, H. Zentgraf, M. Bock, M. Eisenhut, W. Semmler, F. Kiessling, Specific targeting of tumor angiogenesis by RGD-conjugated ultrasmall superparamagnetic iron oxide particles using a clinical 1.5-T magnetic resonance scanner, Cancer Res. 67 (2007) 1555–1562.
[37] N.R. Soman, S.L. Baldwin, G. Hu, J.N. Marsh, G.M. Lanza, J.E. Heuser, J.M. Arbeit, S.A. Wickline, P.H. Schlesinger, Molecularly targeted nanocarriers deliver the cytolytic peptide melittin specifically to tumor cells in mice, reducing tumor growth, J. Clin. Invest. 119 (2009) 2830–2842.
[38] D.B. Kirpotin, D.C. Drummond, Y. Shao, M.R. Shalaby, K. Hong, U.B. Nielsen, J.D. Marks, C.C. Benz, J.W. Park, Antibody targeting of long-circulating lipidic nanoparticles does not increase tumor localization but does increase internalization in animal models, Cancer Res. 66 (2006) 6732–6740.
[39] J.W. Bulte, D.L. Kraitchman, Iron oxide MR contrast agents for molecular and cellular imaging, NMR Biomed. 17 (2004) 484–499.
[40] D.L. Thorek, A.K. Chen, J. Czupryna, A. Tsourkas, Superparamagnetic iron oxide nanoparticle probes for molecular imaging, Ann. Biomed. Eng. 34 (2006) 23–38.
[41] M. Zhao, D.A. Beauregard, L. Loizou, B. Davletov, K.M. Brindle, Non-invasive detection of apoptosis using magnetic resonance imaging and a targeted contrast agent, Nat. Med. 7 (2001) 1241–1244.
[42] M. Mitsunaga, M. Ogawa, N. Kosaka, L.T. Rosenblum, P.L. Choyke, H. Kobayashi, Cancer cell-selective *in vivo* near infrared photoimmunotherapy targeting specific membrane molecules, Nat. Med. 17 (2011) 1685–1691.
[43] E.A. Schellenberger, A. Bogdanov Jr., A. Petrovsky, V. Ntziachristos, R. Weissleder, L. Josephson, Optical imaging of apoptosis as a biomarker of tumor response to chemotherapy, Neoplasia 5 (2003) 187–192.
[44] S. Ke, X. Wen, Q.P. Wu, S. Wallace, C. Charnsangavej, A.M. Stachowiak, C.L. Stephens, J.L. Abbruzzese, D.A. Podoloff, C. Li, Imaging taxane-induced tumor apoptosis using PEGylated, 111In-labeled annexin V, J. Nucl. Med. 45 (2004) 108–115